

www.acsabm.org Forum Article

Reduced Graphene Oxide/Mesoporous Silica Nanocarriers for pH-Triggered Drug Release and Photothermal Therapy

Xiao Liu, Xu Wu,* Yuqian Xing, Ying Zhang, Xuefei Zhang, Qinqin Pu, Min Wu,* and Julia Xiaojun Zhao*



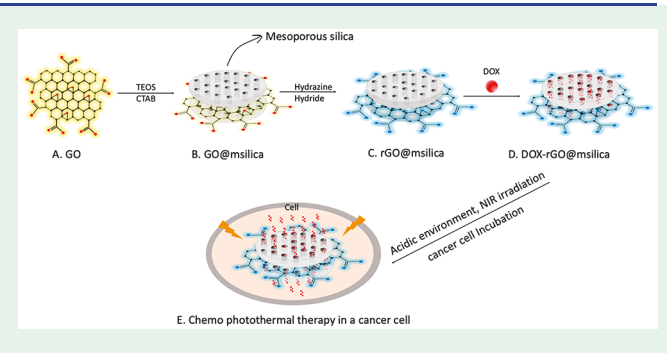
Cite This: https://dx.doi.org/10.1021/acsabm.9b01108



ACCESS

Metrics & More

ABSTRACT: A sandwich structured bifunctional nanocarrier (rGO@msilica) composed of an inner layer of reduced graphene oxide (rGO) and an outer layer of mesoporous silica (msilica) was developed for synergistic chemo-photothermal therapy. The rGO@msilica not only acted as a pH-triggered drug nanocarrier but also worked as a near-infrared (NIR) photothermal agent. The loaded drug, doxorubicin (DOX), in the rGO@msilica nanocarrier was controllably released in the acidic tumor microenvironment. Moreover, the cancer cells were ablated by laser irradiation (808 nm), contributing to the high photothermal conversion efficiency of the rGO core. With this two-in-one system, *in vitro* cancer cell



Article Recommendations

experiments indicated that the synergistic therapeutic strategy was superior to those of single modality therapy. These findings imply that the bifunctional rGO@msilica nanocarrier could provide a powerful platform for cancer therapy.

KEYWORDS: reduced graphene oxide, mesoporous silica, near-infrared, pH-triggered drug release, photothermal therapy

■ INTRODUCTION

Cancer has become a terrifying health threat to human beings worldwide. Up to now, multiple therapeutic strategies have been developed against various cancers. Chemotherapy, considered as one of the most destructive tumor killers, has been widely applied. However, during the period of regular chemo-treatments, passive drug delivery renders considerable side effects to patients, which limit their applications.² Therefore, it is truly urgent to develop a controllable drug release system for effective targeting to malignant tissue regions. Traditional drug carriers generally rely on the blood circulation in the medication process, which is a passive, lacking specificity treatment.^{3,4} Nowadays, active drug delivery systems through certain environmental stimuli, such as light, pH, and thermalization, have been reported. 5-9 Compared with passive targeting drug carriers, the controllable loading and releasing systems execute functions that rely on those internal or external stimulations. As a result, drug targeting efficiency to the pathological cells or tissues would be enhanced significantly, and the healthy cells would be protected.

Among the above-mentioned stimuli-triggered active drug carriers, pH-responsive drug delivery system is an important model in the field of chemotherapy. ¹⁰ In general, cancer cells have a feature of unlimited proliferation, resulting overoxygen consumption and acidic microenvironment compared to healthy tissues. ^{11,12} Consequently, the lower pH value could

be utilized as a stimulus to design active drug delivery carriers for chemotherpy. 10 In this regard, nanomaterials could be applied as a promising active drug carrier¹³ because the functional groups on the nanomaterials could be protonated or deprotonated according to pH of the environment. 14 For example, the carboxyl groups in the polymeric nanocapsules controlled the deformation of nanocapsules. 15 In the basic medium, the carboxyl groups were deprotonated, and the electrostatic attraction between the drug and the carrier limited the drug release. However, in the acidic medium, the carboxyl groups were protonated so that charged molecules had less resistance to transport through the nanocapsules, resulting in the drug release. The charge conversion regulated the loading and releasing behavior of drugs, which implied one of the designations in pH-mediated drug delivery. 16 Using electrostatic interactions to initiate drug release has been considered a major pathway for developing a pH-responsive active drug delivery system.¹⁷

In the development of nanomaterial-based pH-responsive drug delivery systems, several types of nanovehicles have been used including carbon nanotubes, ¹⁸ polymer nanocarriers, ¹⁹

Special Issue: Nucleic Acids: Chemistry, Nanotech-

nology, and Bioapplications

Received: December 2, 2019 Accepted: January 23, 2020



dendrimers, ²⁰ lipids, ^{21,22} gold nanocarriers, ²³ and mesoporous silica nanocarriers. ²⁴ Drugs could be attached on those nanomaterials, loaded into their pores, or encapsulated into vacant domains of nanocarriers. ^{25–27} Among them, mesoporous silica nanocarriers attracted considerable attention due to their decent biocompatibility, easy surface modification, high drug loading efficiency, and good drug release pattern. ²⁸ Accordingly, mesoporous silica is an excellent candidate for drug loading and releasing nanocarriers in cancer therapies. ^{29–34} However, the single modality of chemotherapy with controllable drug loading and releasing properties is not ideal to fulfill the therapeutic efficiency due to the multidrug resistance of cancer.

Multimodal therapeutic strategies have been promoted, especially with the help of multifunctional nanomaterials.³⁵ By combining different therapeutic modalities, such as chemotherapy, photodynamic therapy (PDT), photothermal therapy (PTT), radiotherapy, and immunotherapy, the synergistic effect provided an impressive therapeutic outcome. 36-38 PTT is an invasive, convenient, and promising physical treatment for tumor cells. Several synthesized and modified high-quality photothermal agents have been studied for PTT. ^{39,40} Graphene-based nanomaterials, especially reduced graphene oxide (rGO), have been used for PTT due to its high photothermal conversion efficiency. 41-44 For example, rGO that was coated with a temperature-responsive polymer layer has been successfully applied in a controllable drug release system triggered by a near-infrared (NIR) irradiation. 45 Besides, Zhang et al. selected a polymer layer to wrap graphene oxide, forming a stable and biocompatible photothermal agent. 42 Inspired by these works, we designed a bifunctional nanocarrier using mesoporous silica coated with reduced graphene oxide (rGO@msilica) for cancer synergistic treatment. This nanocarrier has two significant advantages compared with the previous works. First, the coating of mesoporous silica on rGO significantly increased the drug loading capacity and led to the stimuli-responsive drug release pattern. Second, the combination of the photothermal therapy of rGO and chemotherapy promoted the cancer treatment efficiency through synergistic effect.

In this work, the designed sandwich structure of rGO@ msilica nanocarrier has chemo-photothermal therapeutic capacity. The inner layer of the rGO served as a photothermal agent owing to its superior NIR absorption and photothermal conversion efficiency.⁴³ In the outer layer, the mesoporous silica acted as a pH-triggered drug carrier. A chemotherapeutic agent, doxorubicin (DOX), was loaded into the mesoporous silica carrier as well as adsorbed onto the rGO via noncovalent interactions at neutral pH environment. In the acidic environment, DOX was gradually released from the nanocarrier to fulfill the chemotherapeutic function. Meanwhile, rGO@msilica showed fabulous PTT effect under a NIR irradiation, generating synergistic therapeutic efficiency for destroying cancer cells. The investigation of the therapeutic efficiency of rGO@msilica showed an enhanced killing efficiency both in SW620 and A549 cells, a breast cancer line and a lung cancer line, respectively.

EXPERIMENTAL SECTION

Chemicals. Graphene oxide aqueous solution (GO, 5.0 mg/mL) was purchased from ACS Materials. The following chemicals, including doxorubicin hydrochloride (DOX, C₂₇H₂₉NO₁₁·HCl, 98%), tetraethyl orthosilicate (TEOS, C₈H₂₀O₄Si, 98%), sodium

hydroxide (NaOH, 98%), hexadecyltrimethylammonium bromide (CTAB, $CH_3(CH_2)_{15}N(Br)-(CH_3)_3$, 96%), dimethyl sulfoxide (DMSO, (CH₂)₂SO, 99.9%), hydrazine hydrate (N₂H₄, 50%–60%) and hydrochloride acid (HCl, 36.5%-38%), ethanol (C₂H₅OH, 99.8%), and 3-(4,5-dimethylthiazol-2-yl)-2,5-diphenyltetrazolium bromide (MTT, C₁₈H₁₆BrN₅S, 98%), were purchased from Sigma-Aldrich Inc. and used as received without further purification. The deionized (DI) water (18.2 M Ω cm) was obtained from a Millipore water purification system. Dulbecco's modified Eagle's medium (DMEM), Leibovitz's L-15 medium (L-15), and 4'-6-diamidino-2phenylindole (DAPI, C₆H₁₅N₅) were purchased from ThermoFisher Scientific Inc. Colon cancer cell line (SW620) was provided by MD Anderson Cancer Center. Lung cancer cell line (A549) was purchased from the American Tissue Culture Collection (ATCC). Both cells were cultured in the School of Medicine and Health Sciences in the University of North Dakota at 37 °C with 5% CO₂.

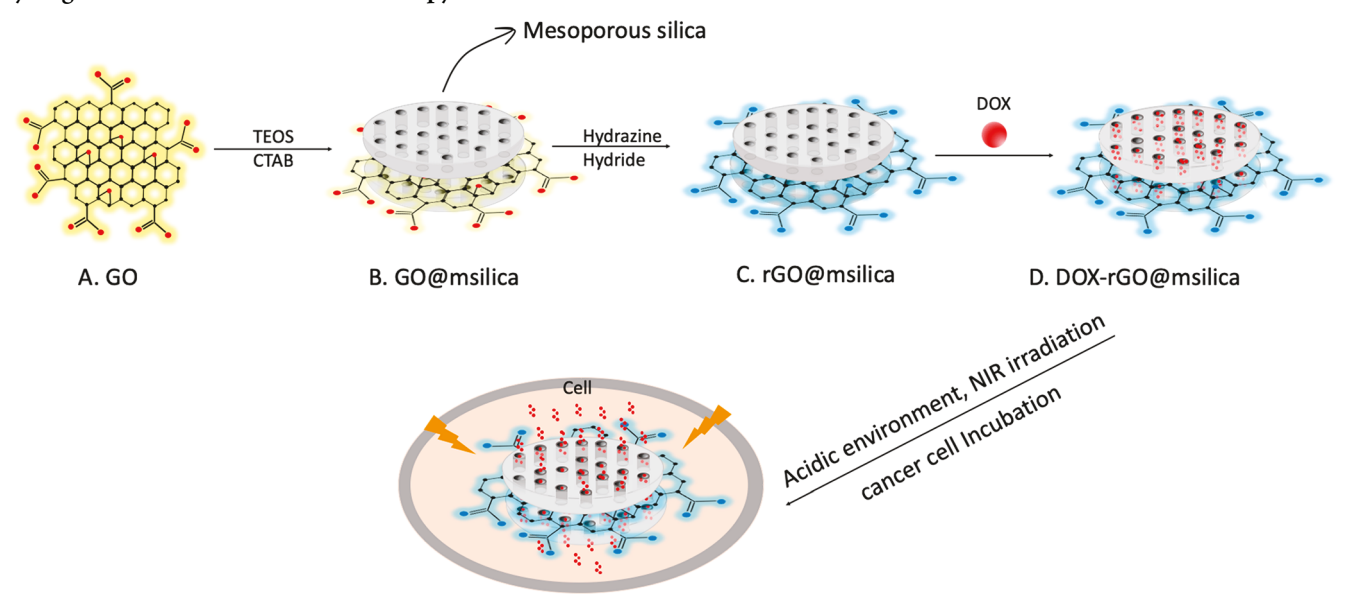
Instruments. An Eppendorf 5804 centrifuge (Eppendorf, Hamburg, BRD) and an ultrasonicator (Branson, Buffalo Grove, IL, USA) were used to separate and disperse nanocarriers. The hydrodynamic diameter and surface potential of the nanocarriers were characterized by the Zetasizer Nano ZS (Marlwen, Worcestershire, UK). A Hitachi SU8010 field emission scanning electron microscope (Hitachi, Tokyo, Japan) was used to take the STEM image of rGO. A Hitachi 7500 transmission electron microscope (Hitachi, Tokyo, Japan) and JEOL JEM-2100 high-resolution transmission electron microscope (JEOL Ltd., Tokyo, Japan) were employed to image the structure of mesoporous silica layer. The pore size and surface area of the nanocarriers were measured by an autosorb-iQ gas sorption analyzer (Quantachrome Instruments, Boynton Beach, FL, USA). The absorption and fluorescence spectra were obtained by a PerkinElmer Lambda 1050 UV-vis/NIR spectrometer (PerkinElmer, Santa Clara, CA, USA) and a Jobin Yvon Horiba Fluorolog-3 spectrofluorometer (Horiba Scientific, Edison, NJ, USA), respectively. A FT-IR Spectrum ATR iD5 spectrometer (ThermoFisher Scientific, Waltham, UK) was used to collect the Fourier transform infrared (FTIR) spectra of the rGO@ msilica. A BWF1 series fiber-coupled diode laser system (808 nm, B&W TEK Inc., Newark, DE, USA) was utilized to irradiate the nanocarrier for executing photothermal therapy. The temperature was monitored with a SK-1250MC electronic thermometer (Sato Keiryoki, Tokyo, Japan). A Multiskan spectrum spectrophotometer (Thermo Fisher Scientific, Waltham, UK) was employed to perform MTT test for measuring the optical density at 570 nm in dimethyl sulfoxide (DMSO) solution.

Synthesis of Reduced Graphene Oxide/Mesoporous Silica Nanocarrier (rGO@msilica). The rGO@msilica nanocarrier was prepared by the following steps. In the beginning, 50.0 mL of deionized water was mixed with 1.0 mL of 5.0 mg/mL GO aqueous solution, followed by sonication for 30 min. The solution was then centrifuged at 7000 rpm for 30 min to remove the precipitant. Afterward, 500 mg of CTAB and 20 mg of sodium hydroxide were added into the previous solution, followed by sonication for 3 h to build a basic condition for hydrolysis of TEOS. Then an aliquot of 250 μ L of TEOS was added into the above solution and stirred for 7 h in a 40 $^{\circ}\text{C}$ water bath. The obtained nanocarrier solution was refluxed in 50 mL of hydrogen chloride (HCl)/ethanol (EtOH) solution (0.1%, v/v) for 3 h to remove the excess CTAB, followed by washing with ethanol and water. The precipitant was redispersed in 50 mL of water. An aliquot of 80 μ L of hydrazine hydride was added and stirred at 100 °C overnight. The final rGO@msilica was washed with water and ethanol (each for three times) and dried in an oven (80 °C) for future usage. The GO@msilica nanocarrier was prepared as a control group following the same procedure mentioned without the reduction process by hydrazine hydride.

Measurement of Pore Size and Surface Area. The obtained dry rGO@msilica nanocarrier was loaded into a 12 mm sample cell in the autosorb-iQ gas sorption analyzer. Before this loading, the weight of the empty sample cell with glass and glass rod was measured. Then the loaded cell was put into a heating mantle for degassing at the temperature of 120 °C for 2 h. After degassing, the sample was

ACS Applied Bio Materials www.acsabm.org Forum Article

Scheme 1. Schematic Illustration of DOX-Loaded rGO@msilica Nanocarrier as Multifunctional Drug Delivery System for Synergetic Chemo-Photothermal Therapy of Cancer



E. Chemo photothermal therapy in a cancer cell

reweighed. Then the loaded cell was transferred into the analysis port. The isotherm curve (volume absorbed vs relative pressure) was plotted, and the pore size and the surface area were obtained.

Measurement of Drug Loading and Releasing Efficiency. An aliquot of 2.0 mL of 1.5 mg/mL rGO@msilica nanocarrier aqueous solution was mixed with 24 µL of 5.0 mg/mL doxorubicin (DOX) and 2.0 mL of 20 mM PBS buffer (pH = 7.4) at room temperature for 24 h. Drug loading efficiency was calculated by measuring the fluorescence intensity of the original solution and the supernatant after centrifugation (11500 rpm, 15 min). Furthermore, the pHdependent drug release behavior of the nanocarrier was investigated under pH 7.4 and pH 5.0. Briefly, two aliquots of 1.0 mL of 0.75 mg/ mL of DOX-loaded rGO@msilica nanocarriers were adjusted to two different pH values, pH 5.0 and pH 7.4, in a PBS buffer. At different time intervals, the solution was centrifuged at 11 500 rpm for 15 min. Then the supernatant was collected for fluorescence measurement, which was used to calculate the amount of DOX with a prepared calibration curve. Similarly, the photoresponsive release of DOX under a NIR irradiation was evaluated in different pH solutions. The initial temperature was adjusted at 37 °C using a water bath. The cuvette was exposed to a NIR diode laser (0.3 W/cm²) for 15 min and cultivated for different period of intervals including 1 h, 2 h, 3 h, 4 h, 5 h, and 6 h.

Photothermal Effect of rGO@msilica. To evaluate the photothermal effect of GO@msilica nanocarrier and rGO@msilica nanocarrier, an aliquot of 2.0 mL of GO@msilica nanocarrier (0.1 mg/mL) and rGO@msilica nanocarrier (0.1 mg/mL) was irradiated with an NIR laser (808 nm, 0.3 W/cm²). The temperature change over time was recorded by an electronic thermometer.

Biocompatibility of rGO@msilica Nanocarrier. A549 lung cancer cells (5.0 \times 10⁴ cells/well) were incubated in a DMEM cell culture medium in a humidified atmosphere with 5% of CO₂ at 37 °C for 24 h. ⁴⁶ The cells were rinsed with a PBS buffer and then treated with different concentrations of unloaded rGO@msilica nanocarriers (0, 2.5, 2.5 \times 10⁻², 2.5 \times 10⁻³, 2.5 \times 10⁻⁴, and 2.5 \times 10⁻⁵ mg/mL) for 24 h in a DMEM medium. The cells were washed to remove the physically adsorbed nanocarriers, and then an MTT solution (5.0 mg/mL, 10 μ L) was subsequently added into each well for incubation of 4.0 h. After the medium was removed, DMSO was added to dissolve the formed formazan violet crystals. The absorbance of formazan in DMSO solution was detected by a microplate reader at 570 nm. A

different cell line (colorectal cancer cells SW620)⁴⁷ has been used to validate the biocompatibility as well.

Chemotherapeutic Effect of DOX-Loaded rGO@msilica Nanocarrier. A549 lung cancer cells $(5.0\times10^4~{\rm cells/well})$ were incubated in DMEM cell culture medium in a humidified atmosphere with 5% of CO₂ at 37 °C for 24 h. Then the cells were treated with different concentrations $(0, 2.5\times10^{-5}, 2.5\times10^{-4}, 2.5\times10^{-3}, 2.5\times10^{-2}, 2.5\times10^{-1}, {\rm and}~2.5~{\rm mg/mL})$ of DOX-loaded rGO@msilica nanocarriers for 12 h in a DMEM medium. An MTT assay was performed to measure the cell viability after the treatment. Furthermore, the impact of incubation time on the cell viability was investigated by MTT assay. Briefly, A549 cells were cultured with DOX loaded rGO@msilica nanocarriers $(25~\mu{\rm g/mL})$ for various time periods $(0, 3, 12, 24, 30, 36, {\rm and}~42~{\rm h})$, followed by the MTT assay to assess the cell viabilities.

Confocal Fluorescence Imaging of Drug Release in Cancer Cells. A549 cells $(2.0 \times 10^5 \text{ cells/well})$ were incubated in the cell culture medium in a humidified atmosphere with 5% of CO₂ at 37 °C for 24 h in a 24-well cell culture plate. Afterward, an aliquot of 500 μ L of DOX-loaded rGO@msilica nanocarrier dispersed in the culture medium $(25 \ \mu\text{g/mL})$ was added into the above cell culture plates. The cells were incubated at 37 °C for 10 min, 6 h, and 24 h, respectively. Cell nuclei were stained by 300 nM DAPI solution. After the cells were washed with PBS buffer to remove the excess DAPI and DOX-loaded rGO@msilica nanocarrier, the fluorescence imaging was taken with a confocal fluorescence microscope.

Synergistic Therapeutic Efficiency. The synergistic therapeutic efficiency of DOX-loaded rGO@msilica nanocarrier was evaluated using A549 cells and SW620 cells. First, the A549 cells (5.0×10^4 cells/well) were seeded on a 96-well plate and cultured for 24 h. Five different treatment groups, including the control group, pure rGO@msilica ($25 \mu g/mL$), DOX-loaded rGO@msilica ($25 \mu g/mL$) with irradiation, and DOX-loaded rGO@msilica ($25 \mu g/mL$) with and irradiation, were used to assess the synergistic therapeutic efficiency. For the irradiation, an 808 nm laser with a power density of 0.3 W/cm² was used for 15 min. After the treatments, the cells were incubated for another 6 or 24 h, followed by the measurement of cell viability using MTT assay. The therapeutic effect was also validated in SW620 cells using the same protocol.

Statistical Analysis. Statistical analysis was performed using Quantachrome ASiQwin software, and Figures were produced using GraphPad Prism 8.0. The significant differences between groups were

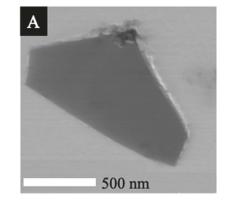
analyzed using student's t test (unpaired and parametric). The quantitative data analysis was manifested as mean \pm standard deviation. Values with p < 0.05 were considered statistically significant (* p < 0.05, ** p < 0.01, *** p < 0.001, *** p < 0.0001).

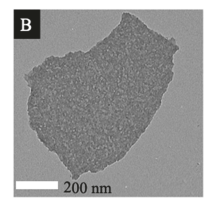
RESULTS AND DISCUSSION

Design and Synthesis of the DOX-Loaded rGO@ msilica Nanocarrier. The design of the bifunctional DOXloaded rGO@msilica nanocarrier was illustrated in Scheme 1. Although the multifunctional drug delivery systems have been developed by many research groups, the DOX-loaded rGO@ msilica nanocarrier developed in this work has the following three main features. First of all, the usage of rGO not only provides a powerful photothermal agent to ablate cancer cells with the irradiation of NIR laser but also works as the controllable drug carrier for DOX. The large sp^2 carbon clusters in rGO efficiently load hydrophobic drugs, like DOX, through $\pi - \pi$ stacking under the normal environment. However, when the environment becomes acidic, the amine groups and carboxyl groups on rGO are protonated, resulting the strong repulsive force between the positive charged DOX and rGO. 50,51 This enhanced repulsive force will trigger the drug release from the nanocarrier. Moreover, under the NIR laser irradiation, the acidic triggered drug releasing efficiency was accelerated by the elevated temperature. Second, the mesoporous silica layers have three important functions in this design. With the protection of the mesoporous silica layers, rGO become more stable than the pure rGO without any modification. Also, the excellent biocompatibility of silica ensures the low cytotoxicity of the nanocarrier for drug delivery. More importantly, the mesopores in the silica layer provide an ideal container for drugs, which could be easily triggered to release in the acidic environment. 52-54 Third, the synergistic effect by the two cancer killing mechanisms, including photothermal ablation and acidic triggered chemotherapy, greatly enhanced the therapeutic efficiency for cancer treatment.

To prepare the nanocarrier, mesoporous silica was first coated on the surface of a single layer GO (Scheme 1A) by the hydrolysis of TEOS with assistance of CTAB in an alkaline environment, forming a sandwich structure (Scheme 1B). Then the inner GO was reduced by hydrazine hydride to form the reduced graphene oxide (rGO, Scheme 1C). Thereafter, a chemotherapeutic drug, doxorubicin hydrochloride (DOX), $^{55-58}$ was loaded into the pores of mesoporous silica layer and the surface of rGO (Scheme 1 D) through electrostatic interaction and π – π stacking. Triggered by the acidic tumor microenvironment, DOX would be released for chemotherapy, which would also be enhanced by the photothermal effect under a NIR laser irradiation (Scheme 1D).

Characterization of DOX-Loaded rGO@msilica Nanocarrier. The morphology and size of rGO@msilica nanocarrier were characterized with a regular transmission electron microscope (TEM) and a high-resolution transmission electron microscope (HRTEM). Without mesoporous silica coating, the pure rGO surface was smooth, and no pores structure was observed (Figure 1A). After the formation of the rGO@msilica sandwich structure, the TEM image (Figure 1B) clearly demonstrated the existence of mesopores silica with the lateral size around 300–500 nm. The HRTEM image (Figure 1C) showed the average pore size of mesoporous silica was about 3 nm. Furthermore, the composition of the synthesized





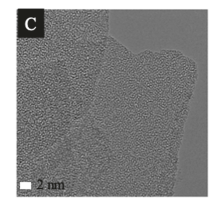
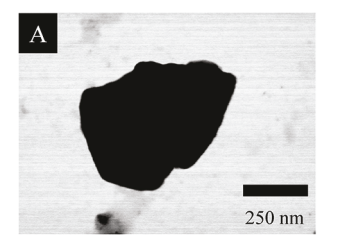
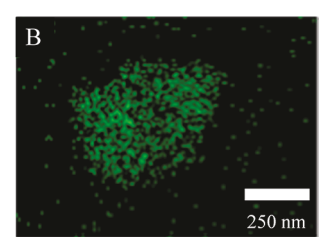
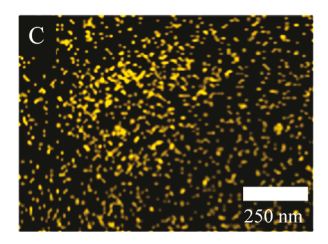


Figure 1. Images of rGO@msilica nanocarrier. (A) STEM image of pure rGO sheet. (B) Low magnification TEM image of rGO@msilica nanocarrier (300–500 nm). (C) HRTEM image of rGO@msilica nanocarrier.

rGO@msilica nanocarriers was investigated using energy-disperse X-ray spectroscopy (EDS) equipped on a SEM. The elemental mapping from EDS showed the overlapping images of elements of C, Si, and O as designed (Figure 2). However, due to the low content of N in the rGO@msilica, no element N map was obtained.







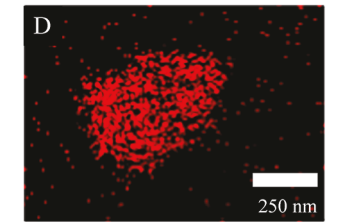


Figure 2. Elemental analysis of the of rGO@msilica nanocarriers. (A) STEM image of the rGO@msilica nanocarrier and its corresponding elemental maps of (B) Si (green color), (C) carbon (yellow color), and (D) oxygen (red color) (scale bar = 250 nm).

The surface area and pore sizes of the rGO@msilica were further measured using a surface area analyzer. The results of N_2 adsorption—desorption isotherm (Figure 3A) and the pore size distribution curve (Figure 3B) indicated that the rGO@msilica nanocarrier possessed a large BET surface area (770 $\rm m^2/g)$. A computational mechanical modeling method, the BJH method (Barrett, Joyner, and Halenda), was employed for calculating the pore size distribution from the experimental isotherms using the Kelvin model of pore filling. The pore volume was 1.21 $\rm cm^2/g$, and the average pore size was estimated as 3.1 nm, which was consistent with the result from the HRTEM images.

To further confirm the formation of the rGO@msilica nanocarrier, we also monitored the absorption spectra (Figure 3C) during the synthetic process. The absorption peaks of GO and GO@msilica nanocarrier were both at 230 nm, which was the characteristic peak of GO. After the reduction, the peak was shifted to 260 nm attributing to the restored sp^2 carbon clusters, indicating the formation of rGO. Meanwhile, the absorbance in the NIR range was significantly enhanced when GO was reduced to rGO, which was useful for PTT using NIR

ACS Applied Bio Materials www.acsabm.org

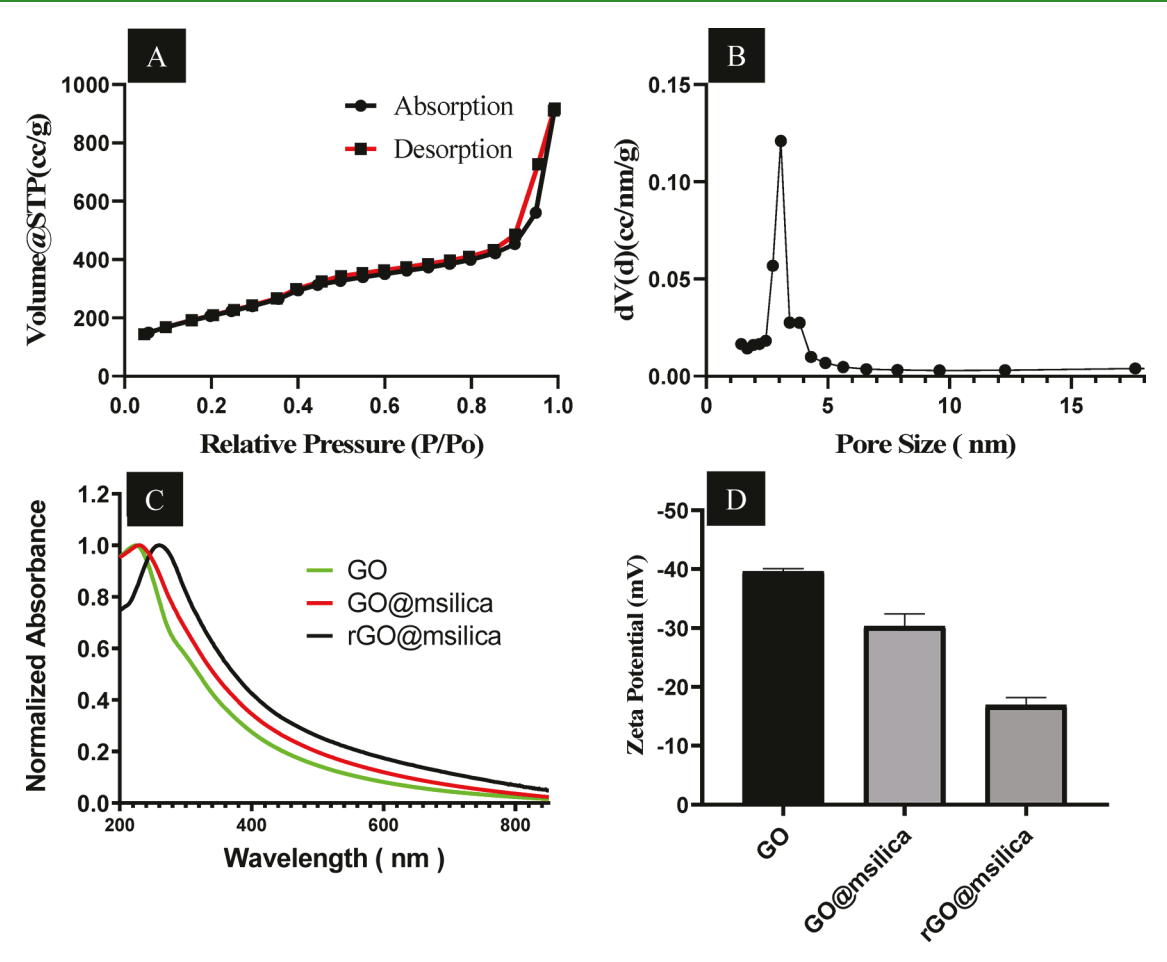


Figure 3. (A) Nitrogen adsorption—desorption isotherm curve and (B) pore size distribution of rGO@msilica nanocarriers based on BJH method. The outgas was conducted at 120 °C for 1.2 h. (C) Absorption spectra of GO, GO@msilica, and rGO@msilica nanocarrier. (D) Zeta potential of GO, GO@msilica, and rGO@msilica nanocarrier in pH 5.0, 10 mM PBS buffer at room temperature.

laser. Moreover, zeta potentials of GO, GO@msilica, and rGO@msilica nanocarrier were measured, which were -39.6 ± 0.5 mV, -30.3 ± 2.1 mV, and -16.8 ± 1.3 mV, respectively (Figure 3D). By coating GO with mesoporous silica, the zeta potential decreased but kept relatively large negative charge due to -OH groups on silica surface. With the formation of rGO, the surface oxygen-containing groups of GO were partially removed, resulting in the further decrease of the zeta potential. Overall, the negative charge surface of rGO@msilica nanocarrier ensured the good stability of the nanocarrier in buffer and medium for bioapplications.

Drug Loading. One of the most important criteria for a successful stimuli-responsive drug delivery platform is that the loaded drug should be released only under the desired conditions with minimal nonspecific leakage. Because of the strong fluorescence of DOX, we used the fluorescence intensity of DOX to measure the loading efficiency and monitor the drug releasing behavior. To avoid false signals caused by the fluorescence variation of DOX, we first studied the pH effect on the fluorescence intensity of the pure DOX molecules. The results showed that DOX was insensitive to pH in the range of 2 to 8 (Figure 4A).

The pH insensitive feature of DOX ensured the accuracy of the measurement of DOX by fluorescence intensity in this work. Therefore, a calibration curve based on the concentration of DOX and fluorescence intensity was established to quantify DOX in different environment (Figure 4B). To

calculate the drug loading efficiency, a certain amount of DOX was loaded to the rGO@msilica nanocarrier as described in the Experimental Section. The drug loading efficiency was measured by the detection of the fluorescence intensities of the initial pure DOX solution (Figure 4C, curve a) and the supernatant after centrifuging the DOX-loaded rGO@msilica nanocarrier (Figure 4C, curve b). The loading efficiency was calculated to be 90%, and the loading amount was 36.0 mg DOX/g nanocarrier. Interestingly, after loading DOX into rGO@msilica nanocarrier, the fluorescence of DOX was strongly quenched by rGO due to its universal fluorescence quenching ability, indicating the successful drug loading. As shown in Figure 4D, the fluorescence intensity of DOX-loaded rGO@msilica was only 1% of the original pure DOX solution.

pH-Responsive Drug Release. Upon the successful loading of DOX into the rGO@msilica nanocarrier, the feature of the pH-triggered drug release behavior was investigated. Two pH values, including pH 7.4 and pH 5.0, were selected for the investigation. By monitoring the fluorescence intensity changes of the supernatant of the DOX-loaded rGO@msilica nanocarriers after centrifugation, the amount of released DOX was measured. As shown in Figure 5A, only 4.8% of the loaded DOX was released in the PBS buffer with pH 7.4 without NIR laser irradiation in the first 6 h. In contrast, a significant large amount of DOX (38.0%) was released from the DOX-loaded rGO@msilica nanocarrier when the pH was changed to 5.0,

Forum Article

ACS Applied Bio Materials

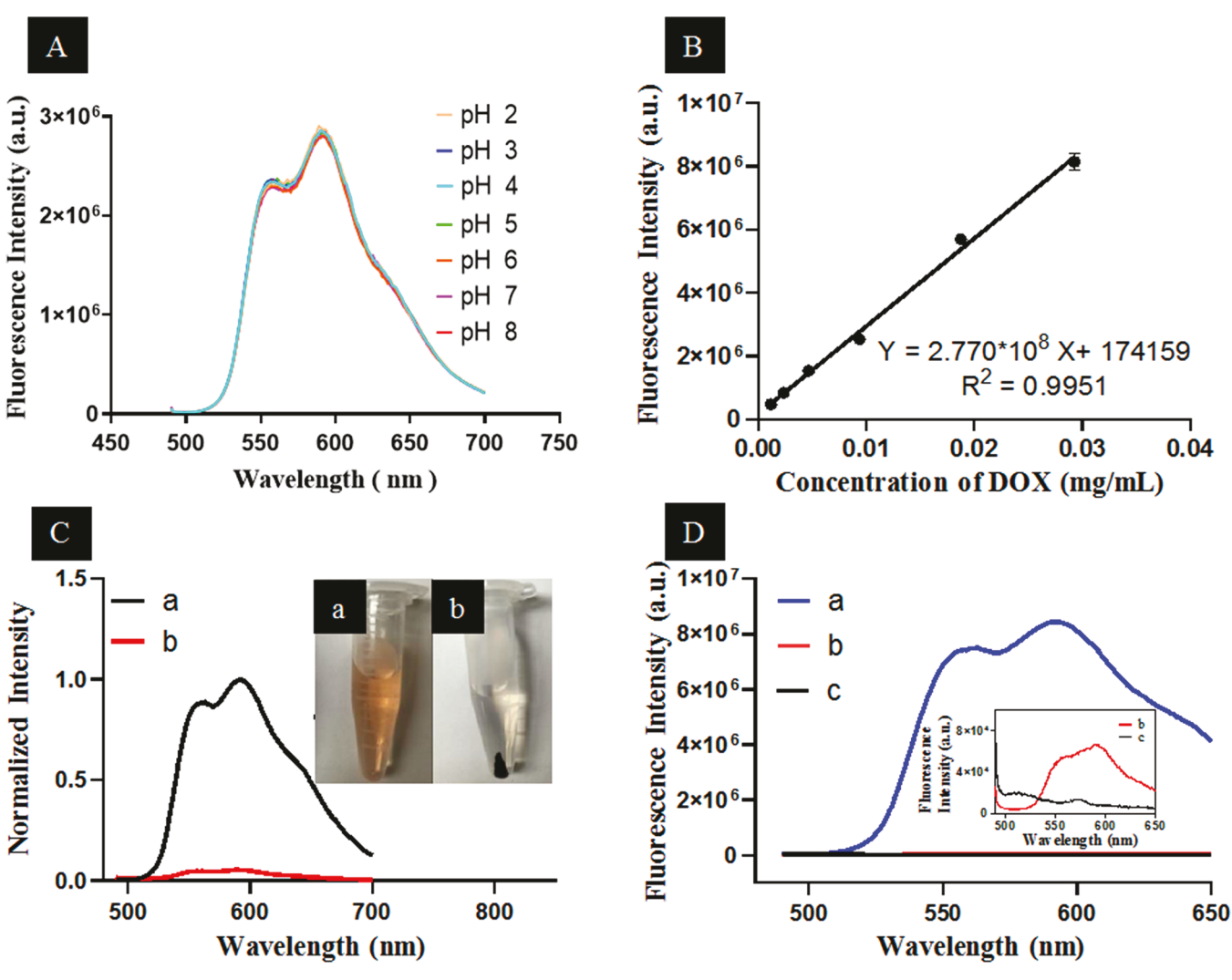


Figure 4. DOX loading into rGO@msilica nanocarrier. (A) Fluorescence spectra of DOX (0.01 mg/mL) at different pH values. (B) Calibration curve of DOX in 10 mM pH 7.4 PBS buffer (DOX concentration: 3.0×10^{-2} , 2.0×10^{-2} , 1.0×10^{-2} , 5.0×10^{-3} , 2.5×10^{-3} , 1.3×10^{-3} mg/mL). (C) Fluorescence spectra of (a) initial pure DOX solution to be used for loading and (b) supernatant after centrifuging DOX-loaded rGO@msilica nanocarrier. Inset shows the (a) initial pure DOX solution and (b) DOX-loaded rGO@msilica nanocarrier solution after centrifugation. (D) Fluorescence spectra of (a) pure DOX (3.0×10^{-2} mg/mL), (b) 7.5×10^{-1} mg/mL DOX-loaded rGO@msilica nanocarriers (with equivalent DOX concentration of 2.7×10^{-2} mg/mL) in 10 mM pH 7.4 PBS buffer, and (c) pure 10 mM pH 7.4 PBS buffer solution as control. Excitation wavelength: 480 nm. Emission wavelength: 591 nm.

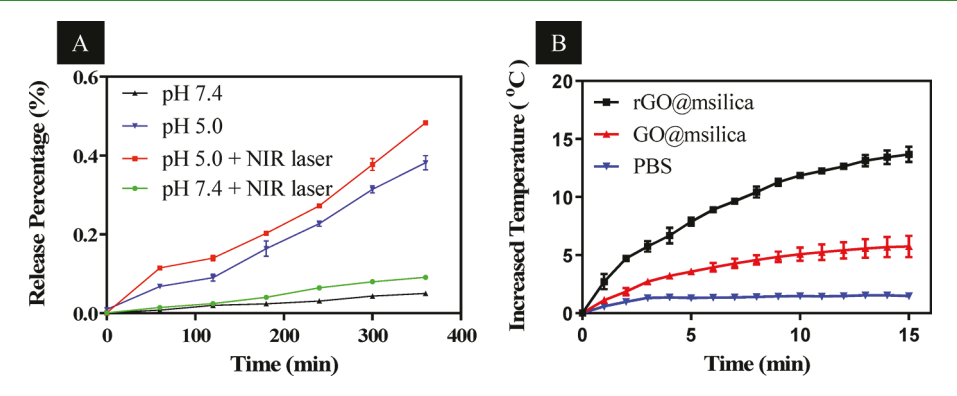


Figure 5. (A) Cumulative release of DOX from DOX-loaded rGO@msilica (0.75 mg/mL) within different pH buffers with or without irradiation. An NIR laser (808 nm, 0.3 W/cm²) was used for irradiation. (B) Temperature increasing curves of PBS, GO@msilica nanocarrier (0.5 mg/mL), and rGO@msilica nanocarrier (0.5 mg/mL) solutions exposed to an NIR laser (808 nm, 0.3 W/cm²) for 15 min. The solution volume was 2.0 mL.

indicating the accelerated drug releasing profile triggered by the acidic environment. Because of the enhanced NIR absorbance of rGO@msilica nanocarrier and the reported PTT effect of rGO, we also investigated the temperature change of the rGO@msilica nanocarrier under the 808 nm laser irradiation. The temperature of the rGO@msilica nanocarrier solution was monitored under the irradiation of an 808 nm laser (0.3 W/cm²) for 15 min (Figure 5B). Without the nanocarrier, the temperature of the PBS increased less than 0.5 °C under the same irradiation (Figure 5B). In contrast, the temperature changes of GO@ msilica nanocarrier solution (0.5 mg/mL) only elevated 4 °C (Figure 5B). Significantly, the temperature changes of the rGO@msilica nanocarrier solution (0.5 mg/mL) exceeded 14 °C (Figure 5B) with the irradiation. The enhanced temperature change of rGO@msilica nanocarrier was higher than that of GO@msilica nanocarrier because the NIR absorbance of rGO was much higher than that of GO at 808 nm (Figure 3C), inducing superior photothermal effect. Considering the normal human body temperature is about 37 °C, the final temperature caused by rGO@msilica with irradiation could be over 51 °C, which would be high enough to kill most of the malignant cells.

More importantly, we proposed that the acid-triggered drug releasing rate would be increased attributing to the enhanced diffusion speed at a higher temperature. Therefore, the drugreleasing profile of DOX-loaded rGO@msilica nanocarrier was also investigated under the laser irradiation in different pH solutions. We first tested irradiation-triggered DOX releasing profile of DOX-loaded rGO@msilica nanocarrier in pH 7.4 solution. As shown in Figure 5A, 9.1% of the loaded DOX was released in the first 6 h with NIR irradiation. Compared to the one without NIR irradiation, an additional of 4.2% drug release was obtained. When the acidic pH of 5.0 was utilized with the NIR irradiation to trigger the drug release, 48.3% of DOX was released from the nanocarrier in 6 h (Figure 5A), which was significantly higher than the single trigger of acidic pH or NIR laser irradiation. Therefore, with the highly efficient photothermal effect, rGO@msilica nanocarrier was expected not only to work as a photothermal agent to directly kill cancer cells but also to possess higher drug release rate with the elevated temperature under the NIR irradiation.

Biocompatibility of rGO@msilica Nanocarriers. The biocompatibility of the nanocarrier was investigated before the application of the nanocarrier for drug delivery. Two cancer cell lines, including human lung cancer cell line (A549) and human colorectal carcinoma cell line (SW620), were selected for this study because of their widespread prevalence and high mortality. As described in the Experimental Section, the cells were incubated with different concentrations of rGO@msilica nanocarrier without loading DOX. After 24 h of incubation, an MTT assay was performed to evaluate the cell viability of these two cell lines. As shown in Figure 6, the cells showed high viability of 84.7% with SW620 and 95.6% with A549 even at the concentration of 2.5 mg/mL. There was no significant difference between different treatment groups (* p < 0.05), indicating the excellent biocompatibility of the rGO@msilica nanocarrier.

Chemotherapy Evaluation of DOX-Loaded rGO@msilica Nanocarrier. Because of the excellent biocompatibility of the rGO@msilica nanocarrier, the chemotherapy of the DOX-loaded rGO@msilica nanocarrier was investigated *in vitro*. A549 lung cancer cells were incubated with different concentrations of DOX-Loaded rGO@msilica (2.5 × 10⁻⁵ to 2.5 mg/mL) for 12 h, followed by the MTT assay to evaluate the cell viability. As shown in Figure 7A, when the concentration of the DOX-Loaded rGO@msilica increased, the cell viability decreased significantly. And 80.4% of the

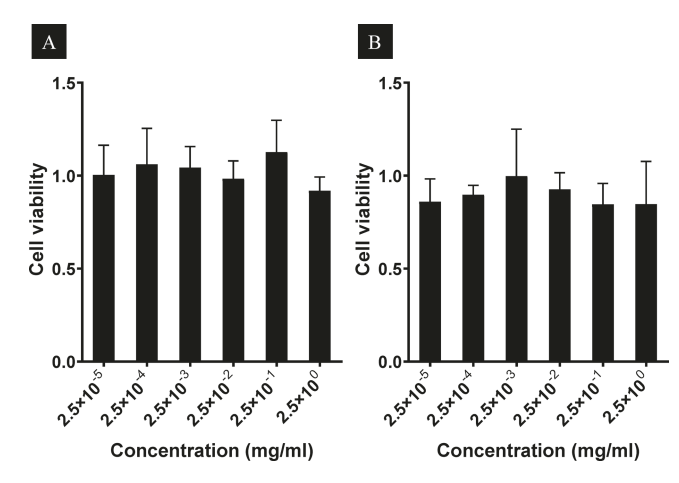


Figure 6. Cell viability of (A) A549 cells and (B) SW620 cells after the treatments with various concentrations of rGO@msilica nanocarriers for 24 h.

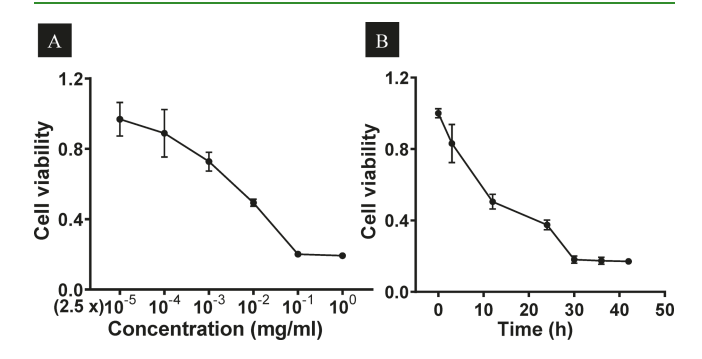


Figure 7. (A) Cell viability of the A549 cells with different concentrations of DOX-loaded rGO@msilica nanocarrier. The concentration of DOX loaded rGO@msilica was from 2.5×10^{-5} mg/mL to 2.5 mg/mL. The incubation time was 12 h. (B) Time effect of the DOX-loaded rGO@msilica nanocarrier on the cell viability of the A549 cells. The concentration of the DOX-loaded rGO@msilica nanocarrier was 2.5×10^{-2} mg/mL.

cancer cells were killed when the concentration of DOX-loaded rGO@msilica nanocarrier reached 2.5 mg/mL. The results demonstrated a dose-dependent therapeutic effect of the DOX-loaded rGO@msilica nanocarrier to the A549 cancer cells. The IC $_{50}$ concentration was calculated to be 2.5×10^{-2} mg/mL at the period of 12-h incubation. The effect of the incubation period on the A549 cell viability was also investigated at the concentration of 2.5×10^{-2} mg/mL. As shown in Figure 7B, the A549 cell viability decreased as the time collapsed and reached the plateau at 30 h. At this moment, 82.9% of cancer cells were killed, and the same value remained as the time increased to 40 h. The result indicated that the drug release from the rGO@msilica nanocarrier was a slow and effective process.

Cellular Uptake and Drug Release in Cells. To further confirm the drug release behavior of the nanocarrier in cancer cells, confocal fluorescence images of A549 cells were taken under different incubation time periods with the DOX-loaded rGO@msilica nanocarrier (Figure 8A). The cells were also stained with DAPI²³ as it could bind with DNAs to show strong blue fluorescence. When the DOX-loaded rGO@msilica nanocarrier $(2.5 \times 10^{-2} \text{ mg/mL})$ was incubated with cells for only 10 min, the fluorescence signal from DOX was mainly localized around the nucleus (Figure 8A), which was because

ACS Applied Bio Materials www.acsabm.org Forum Article

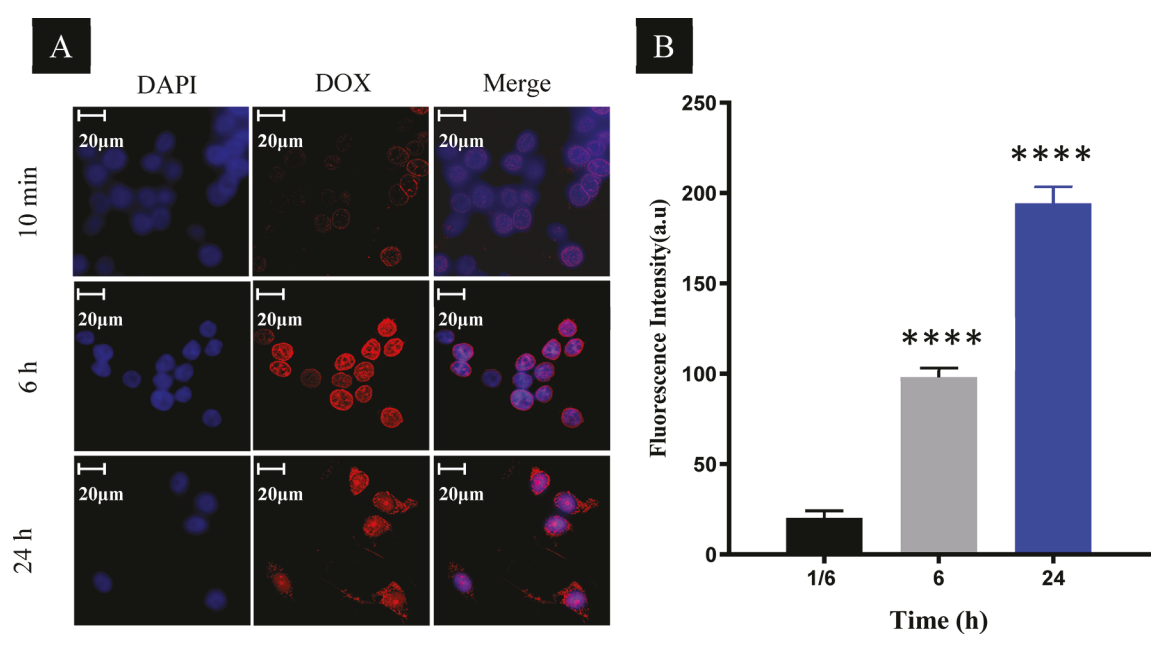


Figure 8. (A) Confocal fluorescence images of A549 cells incubated with DOX-loaded rGQ@msilica nanocarrier at different time periods, including 10 min, 6 h, and 24 h. The nucleus was counterstained with DAPI (blue). The red fluorescence was from DOX. (B) Fluorescence intensity of DOX in cells was quantified by ImageJ software (**** p < 0.0001).

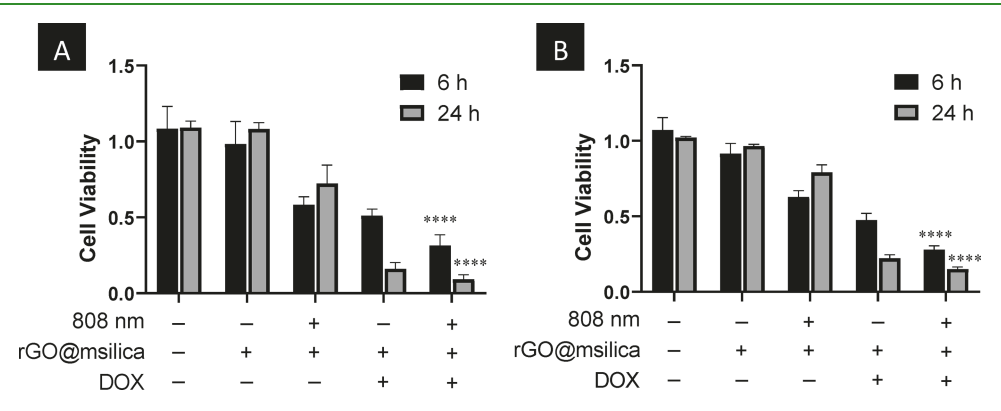


Figure 9. Cell viabilities of (A) SW620 and (B) A549 cells after different treatments. "-" stands for no treatment. "+" stands for the treatment. The cells were incubated with nanocarriers for 6 and 24 h, respectively, followed by the 808 nm laser irradiation of 15 min (**** p < 0.0001).

the unreleased DOX from the nanocarrier could not enter the nucleus with the relative large size of the nanocarrier. However, when the incubation time increased to 6 h, most of the DOX fluorescence was colocalized with DAPI in the nucleus (Figure 8A), indicating the effective drug release from the nanocarrier. When the incubation time increased to 24 h, the red fluorescence spread in both nucleus and cytoplasm due to the drug release from the nanocarrier. The intensities of these fluorescence signals were quantitatively measured (Figure 8B). The red fluorescence from DOX was gradually enhanced in cells with time, indicating the gradually drug release in cells.

Synergistic Chemo-Photothermal Therapy of Cancer Cells. As previously discussed, rGO was well recognized as an efficient photothermal agent for cancer treatment. Combined with the chemotherapy of the loaded DOX, the synergistic chemo-photothermal therapeutic effect of the DOX-loaded rGO@msilica nanocarrier was investigated under an NIR irradiation (808 nm, 0.3 W/cm²). As shown in Figure 9, SW620 cells (Figure 9A) and A549 cells (Figure 9B) were incubated with 2.5×10^{-2} mg/mL DOX-loaded rGO@msilica nanocarrier for 6 and 24 h, followed by the NIR laser

irradiation (808 nm, 0.3 W/cm²) for 15 min. Then the cells were cultured in medium for additional 12 h, followed by the MTT assay to assess the cell viabilities. The results showed that pure rGO@msilica nanocarrier has no significant cytotoxic activity to both cell lines compared with the control group, indicating the great biocompatibility of the rGO@msilica nanocarrier. Take SW620 cells as an example, the photothermal therapy effect caused by the combination of the rGO@msilica nanocarrier and NIR laser irradiation showed a moderate therapeutic effect, which resulted in the reduction of cell viability to 60% and 66% at 6 and 24 h, respectively. Moreover, the cell viability of SW620 cells treated with DOXloaded rGO@msilica nanocarrier without NIR irradiation caused severe cell death, resulting in the cell viabilities of 51% and 19% at 6 and 24 h, respectively. More importantly, the combination of the chemo-photothermal therapy by treating cells with DOX-loaded rGO@msilica nanocarrier and NIR irradiation killed more cells. At 6 and 24 h, the cell viabilities decreased to 31% and 9%, respectively. Similarly, the synergistic therapeutic efficiency was demonstrated in the treatment of A549 cells (Figure 9B). Thus, DOX-loaded

rGO@msilica nanocarrier composed of chemo-photothermal therapeutic capacities demonstrates better antitumor efficiency compared to a single modal therapy.

CONCLUSIONS

In summary, we have designed and constructed a bifunctional DOX-loaded rGO@msilica nanocarrier with photothermal effect and pH-responsive drug release properties. The large surface area and pore size of the rGO@msilica nanocarrier possessed effectively drug loading efficiency and pH-responsive drug releasing behavior. Moreover, in the acidic environment with NIR irradiation, the drug releasing efficiency was significantly enhanced, causing significant cancer cell death. The synergetic effect of chemotherapy and photothermal therapy under NIR irradiation demonstrated the enhanced cancer cell killing efficacy in vitro. The developed rGO@msilica nanocarriers might have great potential for fighting cancer by the combined therapeutic strategies.

AUTHOR INFORMATION

Corresponding Authors

Xu Wu – Department of Chemistry, University of North Dakota, Grand Forks, North Dakota 58202, United States;

orcid.org/0000-0003-1336-9571; Email: Xu.wu@und.edu

Min Wu — Department of Biomedical Sciences, School of Medicine and Health Science, University of North Dakota, Grand Forks, North Dakota 58202, United States; Email: Min.wu@med.und.edu

Julia Xiaojun Zhao — Department of Chemistry, University of North Dakota, Grand Forks, North Dakota 58202, United States; oorcid.org/0000-0002-9603-666X; Email: Julia.zhao@und.edu

Authors

Xiao Liu — Department of Chemistry, University of North Dakota, Grand Forks, North Dakota 58202, United States
Yuqian Xing — Department of Chemistry, University of North Dakota, Grand Forks, North Dakota 58202, United States
Ying Zhang — Department of Chemistry, University of North Dakota, Grand Forks, North Dakota 58202, United States
Xuefei Zhang — Department of Chemistry, University of North Dakota, Grand Forks, North Dakota 58202, United States
Qinqin Pu — Department of Biomedical Sciences, School of Medicine and Health Science, University of North Dakota, Grand Forks, North Dakota 58202, United States

Complete contact information is available at: https://pubs.acs.org/10.1021/acsabm.9b01108

Notes

The authors declare no competing financial interest.

■ ACKNOWLEDGMENTS

This work was supported by the NSF grant CHE 1709160 (J.X.Z.) and North Dakota Industrial Commission (G-041-081, J.X.Z.) as well as NIH AI138203-02 and AI109317-05 (M.W.). The authors acknowledge the use of the Edward C. Carlson Imaging and Image Analysis Core Facility, which is supported in part by NIH grants 1P20GM113123 and P20GM103442.

REFERENCES

(1) Poutahidis, T.; Varian, B. J.; Levkovich, T.; Lakritz, J. R.; Mirabal, S.; Kwok, C.; Ibrahim, Y. M.; Kearney, S. M.; Chatzigiagkos,

- A.; Alm, E. J.; Erdman, S. E. Dietary Microbes Modulate Transgenerational Cancer Risk. *Cancer Res.* **2015**, *75*, 1197–1204.
- (2) Lukianova-Hleb, E. Y.; Ren, X.; Zasadzinski, J. A.; Wu, X.; Lapotko, D. O. Plasmonic Nanobubbles Enhance Efficacy and Selectivity of Chemotherapy Against Drug-Resistant Cancer Cells. *Adv. Mater.* **2012**, *24*, 3831–3837.
- (3) Danhier, F.; Feron, O.; Préat, V. To Exploit the Tumor Microenvironment: Passive and Active Tumor Targeting of Nanocarriers for Anti-cancer Drug Delivery. *J. Controlled Release* **2010**, *148*, 135–146.
- (4) Bae, Y. H.; Park, K. Targeted Drug Delivery to Tumors: Myths, Reality and Possibility. *J. Controlled Release* **2011**, *153*, 198–205.
- (5) Theato, P.; Sumerlin, B. S.; O'Reilly, R. K.; Epps, I. I. I. T. H. Stimuli Responsive Materials. *Chem. Soc. Rev.* **2013**, *42*, 7055–7056.
- (6) Wang, H.; Zhao, S.; Agarwal, P.; Dumbleton, J.; Yu, J.; Lu, X.; He, X. Multi-layered Polymeric Nanoparticles for pH-responsive and Sequenced Release of Theranostic Agents. *Chem. Commun.* **2015**, *51*, 7733–7736.
- (7) Dai, Y.; Ma, P. a.; Cheng, Z.; Kang, X.; Zhang, X.; Hou, Z.; Li, C.; Yang, D.; Zhai, X.; Lin, J. Up-Conversion Cell Imaging and pH-Induced Thermally Controlled Drug Release from NaYF₄:Yb³⁺/Er³⁺@Hydrogel Core—Shell Hybrid Microspheres. *ACS Nano* **2012**, *6*, 3327–3338.
- (8) Brannon-Peppas, L.; Blanchette, J. O. Nanoparticle and Targeted Systems for Cancer Therapy. *Adv. Drug Delivery Rev.* **2004**, *56*, 1649–1659
- (9) Mitragotri, S.; Lahann, J. Materials for Drug Delivery: Innovative Solutions to Address Complex Biological Hurdles. *Adv. Mater.* **2012**, 24, 3717–3723.
- (10) Gao, W.; Chan, J. M.; Farokhzad, O. C. pH-Responsive Nanoparticles for Drug Delivery. *Mol. Pharmaceutics* **2010**, *7*, 1913–1920.
- (11) Estrella, V.; Chen, T.; Lloyd, M.; Wojtkowiak, J.; Cornnell, H. H.; Ibrahim-Hashim, A.; Bailey, K.; Balagurunathan, Y.; Rothberg, J. M.; Sloane, B. F.; Johnson, J.; Gatenby, R. A.; Gillies, R. J. Acidity Generated by The Tumor Microenvironment Drives Local Invasion. *Cancer Res.* 2013, 73, 1524–1535.
- (12) Kato, Y.; Ozawa, S.; Miyamoto, C.; Maehata, Y.; Suzuki, A.; Maeda, T.; Baba, Y. Acidic Extracellular Microenvironment and Cancer. *Cancer Cell Int.* **2013**, *13*, 89–89.
- (13) Zheng, Y.; Wang, L.; Lu, L.; Wang, Q.; Benicewicz, B. C. pH and Thermal Dual-Responsive Nanoparticles for Controlled Drug Delivery with High Loading Content. ACS Omega 2017, 2, 3399—3405.
- (14) Esfand, R.; Tomalia. Poly(amidoamine) (PAMAM) Dendrimers: from Biomimicry to Drug Delivery and Biomedical Applications. *Drug Discovery Today* **2001**, *6*, 427–436.
- (15) Hu, H.; Zhang, X.; Sun, J.; An, L.; Du, J.; Yang, H.; Li, F.; Wu, H.; Yang, S. Preparation of pH-Responsive Hollow Poly(MAA-co-EGDMA) Nanocapsules for Drug Delivery and Ultrasound Imaging. RSC Adv. 2016, 6, 103754–103762.
- (16) Dergunov, S. A.; Durbin, J.; Pattanaik, S.; Pinkhassik, E. pH-Mediated Catch and Release of Charged Molecules with Porous Hollow Nanocapsules. *J. Am. Chem. Soc.* **2014**, *136*, 2212–2215.
- (17) Pan, A. C.; Borhani, D. W.; Dror, R. O.; Shaw, D. E. Molecular Determinants of Drug-receptor Binding Kinetics. *Drug Discovery Today* **2013**, *18*, 667–673.
- (18) Pascu, S. I.; Arrowsmith, R. L.; Bayly, S. R.; Brayshaw, S.; Hu, Z. Towards Nanomedicines: Design Protocols to Assemble, Visualize and Test Carbon Nanotube Probes for Multi-modality Biomedical Imaging. *Philos. Trans. R. Soc., A* **2010**, *368*, 3683–3712.
- (19) Hans, M. L.; Lowman, A. M. Biodegradable Nanoparticles for Drug Delivery and Targeting. *Curr. Opin. Solid State Mater. Sci.* **2002**, 6, 319–327.
- (20) Pistolis, G.; Malliaris, A.; Tsiourvas, D.; Paleos, C. M. Poly(propyleneimine) Dendrimers as pH-Sensitive Controlled-Release Systems. *Chem. Eur. J.* **1999**, *5*, 1440–1444.

I

- (21) Yatvin, M. B.; Kreutz, W.; Horwitz, B. A.; Shinitzky, M. pH-sensitive Liposomes: Possible Clinical Implications. *Science* **1980**, *210*, 1253–1255.
- (22) Gujrati, M.; Vaidya, A.; Lu, Z.-R. Multifunctional pH-Sensitive Amino Lipids for siRNA Delivery. *Bioconjugate Chem.* **2016**, 27, 19–35.
- (23) Nam, J.; La, W.-G.; Hwang, S.; Ha, Y. S.; Park, N.; Won, N.; Jung, S.; Bhang, S. H.; Ma, Y.-J.; Cho, Y.-M.; Jin, M.; Han, J.; Shin, J.-Y.; Wang, E. K.; Kim, S. G.; Cho, S.-H.; Yoo, J.; Kim, B.-S.; Kim, S. pH-Responsive Assembly of Gold Nanoparticles and "Spatiotemporally Concerted" Drug Release for Synergistic Cancer Therapy. *ACS Nano* 2013, 7, 3388–3402.
- (24) He, Q.; Gao, Y.; Zhang, L.; Zhang, Z.; Gao, F.; Ji, X.; Li, Y.; Shi, J. A pH-responsive Mesoporous Silica Nanoparticles-based Multi-drug Delivery System for Overcoming Multi-drug Resistance. *Biomaterials* **2011**, *32*, 7711–7720.
- (25) Bharti, C.; Nagaich, U.; Pal, A. K.; Gulati, N. Mesoporous Silica Nanoparticles in Target Drug Delivery System: A review. *Int. J. Pharm. Investig.* **2015**, *5*, 124–133.
- (26) Karimi, M.; Ghasemi, A.; Sahandi Zangabad, P.; Rahighi, R.; Moosavi Basri, S. M.; Mirshekari, H.; Amiri, M.; Shafaei Pishabad, Z.; Aslani, A.; Bozorgomid, M.; Ghosh, D.; Beyzavi, A.; Vaseghi, A.; Aref, A. R.; Haghani, L.; Bahrami, S.; Hamblin, M. R. Smart Micro/Nanoparticles in Stimulus-Responsive Drug/Gene Delivery Systems. *Chem. Soc. Rev.* **2016**, *45*, 1457–1501.
- (27) Manzano, M.; Vallet-Regi, M. New Developments in Ordered Mesoporous Materials for Drug Delivery. *J. Mater. Chem.* **2010**, 20, 5593–5604.
- (28) Yang, P.; Gai, S.; Lin, J. Functionalized Mesoporous Silica Materials for Controlled Drug Delivery. *Chem. Soc. Rev.* **2012**, *41*, 3679–3698.
- (29) Pan, L.; He, Q.; Liu, J.; Chen, Y.; Ma, M.; Zhang, L.; Shi, J. Nuclear-Targeted Drug Delivery of TAT Peptide-Conjugated Monodisperse Mesoporous Silica Nanoparticles. *J. Am. Chem. Soc.* **2012**, *134*, 5722–5725.
- (30) Kwon, S.; Singh, R. K.; Perez, R. A.; Abou Neel, E. A.; Kim, H.-W.; Chrzanowski, W. Silica-based Mesoporous Nanoparticles for Controlled Drug Delivery. *J. Tissue Eng.* **2013**, *4*, 2041731413503357.
- (31) Watermann, A.; Brieger, J. Mesoporous Silica Nanoparticles as Drug Delivery Vehicles in Cancer. *Nanomaterials* **2017**, *7*, 189.
- (32) Hao, X.; Hu, X.; Zhang, C.; Chen, S.; Li, Z.; Yang, X.; Liu, H.; Jia, G.; Liu, D.; Ge, K.; Liang, X.-J.; Zhang, J. Hybrid Mesoporous Silica-Based Drug Carrier Nanostructures with Improved Degradability by Hydroxyapatite. ACS Nano 2015, 9, 9614–9625.
- (33) Yuan, L.; Tang, Q.; Yang, D.; Zhang, J. Z.; Zhang, F.; Hu, J. Preparation of pH-Responsive Mesoporous Silica Nanoparticles and Their Application in Controlled Drug Delivery. *J. Phys. Chem. C* **2011**, *115*, 9926–9932.
- (34) Zhang, G.; Yang, M.; Cai, D.; Zheng, K.; Zhang, X.; Wu, L.; Wu, Z. Composite of Functional Mesoporous Silica and DNA: An Enzyme-Responsive Controlled Release Drug Carrier System. ACS Appl. Mater. Interfaces 2014, 6, 8042–8047.
- (35) Fan, W.; Yung, B.; Huang, P.; Chen, X. Nanotechnology for Multimodal Synergistic Cancer Therapy. *Chem. Rev.* **2017**, *117*, 13566–13638.
- (36) Zhao, Z. X.; Huang, Y. Z.; Shi, S. G.; Tang, S. H.; Li, D. H.; Chen, X. L. Cancer Therapy Improvement with Mesoporous Silica Nanoparticles Combining Photodynamic and Photothermal Therapy. *Nanotechnology* **2014**, *25*, 285701.
- (37) Yao, X.; Tian, Z.; Liu, J.; Zhu, Y.; Hanagata, N. Mesoporous Silica Nanoparticles Capped with Graphene Quantum Dots for Potential Chemo-Photothermal Synergistic Cancer Therapy. *Langmuir* **2017**, 33, 591–599.
- (38) Hong, E. J.; Choi, D. G.; Shim, M. S. Targeted and Effective Photodynamic Therapy for Cancer Using Functionalized Nanomaterials. *Acta Pharm. Sin. B* **2016**, *6*, 297–307.
- (39) Huang, X.; El-Sayed, I. H.; Qian, W.; El-Sayed, M. A. Cancer Cell Imaging and Photothermal Therapy in the Near-Infrared Region by Using Gold Nanorods. *J. Am. Chem. Soc.* **2006**, *128*, 2115–2120.

- (40) Zhang, Z.; Wang, J.; Nie, X.; Wen, T.; Ji, Y.; Wu, X.; Zhao, Y.; Chen, C. Near Infrared Laser-Induced Targeted Cancer Therapy Using Thermoresponsive Polymer Encapsulated Gold Nanorods. *J. Am. Chem. Soc.* **2014**, *136*, 7317–7326.
- (41) Robinson, J. T.; Tabakman, S. M.; Liang, Y.; Wang, H.; Sanchez Casalongue, H.; Vinh, D.; Dai, H. Ultrasmall Reduced Graphene Oxide with High Near-Infrared Absorbance for Photothermal Therapy. *J. Am. Chem. Soc.* **2011**, *133*, 6825–6831.
- (42) Zhang, W.; Guo, Z.; Huang, D.; Liu, Z.; Guo, X.; Zhong, H. Synergistic Effect of Chemo-photothermal Therapy Using PEGylated Graphene Oxide. *Biomaterials* **2011**, *32*, 8555–8561.
- (43) Cheon, Y. A.; Bae, J. H.; Chung, B. G. Reduced Graphene Oxide Nanosheet for Chemo-photothermal Therapy. *Langmuir* **2016**, 32, 2731–2736.
- (44) Kang, S.; Lee, J.; Ryu, S.; Kwon, Y.; Kim, K.-H.; Jeong, D. H.; Paik, S. R.; Kim, B.-S. Gold Nanoparticle/Graphene Oxide Hybrid Sheets Attached on Mesenchymal Stem Cells for Effective Photothermal Cancer Therapy. *Chem. Mater.* **2017**, *29*, 3461–3476.
- (45) Wang, D.; Duan, H.; Lu, J.; Lu, C. Fabrication of Thermoresponsive Polymer Functionalized Reduced Graphene Oxide@Fe₃O₄@Au Magnetic Nanocomposites for Enhanced Catalytic Applications. *J. Mater. Chem. A* **2017**, *5*, 5088–5097.
- (46) Wang, W.; Ye, Y.; Li, J.; Li, X.; Zhou, X.; Tan, D.; Jin, Y.; Wu, E.; Cui, Q.; Wu, M. Lyn Regulates Cytotoxicity in Respiratory Epithelial Cells Challenged by Cigarette Smoke Extracts. *Curr. Mol. Med.* **2014**, *14*, 663–672.
- (47) Yuan, K.; Xie, K.; Fox, J.; Zeng, H.; Gao, H.; Huang, C.; Wu, M. Decreased Levels of miR-224 and the Passenger Strand of miR-221 Increase MBD2, Suppressing Maspin and Promoting Colorectal Tumor Growth and Metastasis in Mice. *Gastroenterology* **2013**, *145*, 853–864.
- (48) Goenka, S.; Sant, V.; Sant, S. Cancer Therapy Graphene-based Nanomaterials for Drug Delivery and Tissue Engineering. *J. Controlled Release* **2014**, *173*, 75–88.
- (49) Georgakilas, V.; Otyepka, M.; Bourlinos, A. B.; Chandra, V.; Kim, N.; Kemp, K. C.; Hobza, P.; Zboril, R.; Kim, K. S. Functionalization of Graphene: Covalent and Non-Covalent Approaches, Derivatives and Applications. *Chem. Rev.* **2012**, *112*, 6156–6214.
- (50) Na, Y. I.; Song, Y. I.; Kim, S. W.; Suh, S. J. Study on Properties of Eco-friendly Reduction Agents for the Reduced Graphene Oxide Method. *Carbon Lett.* **2017**, *24*, 1–9.
- (51) Wang, R.; Wang, Y.; Xu, C.; Sun, J.; Gao, L. Facile One-step Hydrazine-assisted Solvothermal Synthesis of Nitrogen-doped Reduced Graphene Oxide: Reduction Effect and Mechanisms. *RSC Adv.* **2013**, *3*, 1194–1200.
- (52) Muhammad, F.; Guo, M.; Qi, W.; Sun, F.; Wang, A.; Guo, Y.; Zhu, G. pH-Triggered Controlled Drug Release from Mesoporous Silica Nanoparticles via Intracelluar Dissolution of ZnO Nanolids. *J. Am. Chem. Soc.* **2011**, 133, 8778–8781.
- (53) ALOthman, Z. A Review: Fundamental Aspects of Silicate Mesoporous Materials. *Materials* **2012**, *5*, 2874.
- (54) Cauda, V.; Schlossbauer, A.; Bein, T. Bio-Degradation Study of Colloidal Mesoporous Silica Nanoparticles: Effect of Surface Functionalization with Organo-Silanes and Poly(Ethylene Glycol). *Microporous Mesoporous Mater.* **2010**, *132*, 60–71.
- (55) Smith, L.; Watson, M. B.; O'Kane, S. L.; Drew, P. J.; Lind, M. J.; Cawkwell, L. The Analysis of Doxorubicin Resistance in Human Breast Cancer Cells Using Antibody Microarrays. *Mol. Cancer Ther.* **2006**, *5*, 2115–2120.
- (56) Shen, Z.; Shen, T.; Wientjes, M. G.; O'Donnell, M. A.; Au, J. L. S. Intravesical Treatments of Bladder Cancer: Review. *Pharm. Res.* **2008**, 25, 1500–1510.
- (57) Wang, S.-L.; Lee, J.-J.; Liao, A. T. Comparison of Efficacy and Toxicity of Doxorubicin and Mitoxantrone in Combination Chemotherapy for Canine Lymphoma. *Can. Vet. J.* **2016**, *57*, 271–276.
- (58) Thorn, C. F.; Oshiro, C.; Marsh, S.; Hernandez-Boussard, T.; McLeod, H.; Klein, T. E.; Altman, R. B. Doxorubicin Pathways:

Pharmacodynamics and Adverse Effects. *Pharmacogenet. Genomics* **2011**, *21*, 440–446.